

Solvent dependent formation of Cu(II) complexes based on isonicotinamide ligand

*Francisco Sánchez-Férez^a, Laura Bayés^b, Mercè Font-Bardia^c, José A. Ayllón^a,
Josefina Pons^{a,*}*

^aDepartament de Química, Universitat Autònoma de Barcelona, 08193-Bellaterra,
Barcelona, Spain

^bCristal·lografia, Mineralogia I Dipòsits Minerals, Universitat de Barcelona, Martí i
Franquès s/n, 08028 Barcelona, Spain

^cUnitat de Difracció de Raig-X, Centres Científics i Tecnològics de la Universitat de
Barcelona (CCiYUB), Universitat de Barcelona, Solé i Sabarís, 1-3, 08028 Barcelona,
Spain

Cu(II) complexes; Isonicotinamide ligand; Solvent-controlled formation; X-ray crystal
structures; Supramolecular networks; Hirshfeld surfaces

Abstract

Five solvent-dependent Cu(II) compounds have been synthesized with $[\text{Cu}(\mu\text{-OAc})(\mu\text{-Pip})(\text{MeOH})_2]$ (OAc = acetate; Pip = 1,3-benzodioxolecarboxylate) and isonicotinamide (Isn) as an auxiliary ligand in different solvents. In all compounds the Pip units are displaced resulting in dimeric $[\text{Cu}(\mu\text{-OAc})(\text{OAc})(\text{Isn})_2(\text{solvent})]_2$ (solvent = MeOH (**2a**), dmf and H₂O (**3**) or H₂O and HPip (**4a**)), paddle-wheel $[\text{Cu}(\mu\text{-OAc})_2(\text{Isn})]_2 \cdot 2\text{dmsO}$ (**5**) or monomeric compound $[\text{Cu}(\text{OAc})_2(\text{HOAc})(\text{Isn})_2] \cdot \text{HOAc}$ (**6**). All of them have been characterized by analytical and ATR-FTIR techniques and its X-ray crystal structures are solved. The OAc anions construct different arrays and exhibits different coordination modes depending on the solvent used. The supramolecular expansion is constantly determined by the amide-amide pattern and the role of the occluded solvent molecules. This tendency is confirmed by Hirshfeld Surface analysis. Finally, the thermal stability of compound **4a** is analyzed.

Introduction

The study of the coordination chemistry of Cu(II) complexes with carboxylate groups has a great interest due to their labile nature and versatility. Moreover, the use of Cu(II) ion with d^9 electronic configuration, as metal node, confers different coordination numbers and geometries, varying from tetrahedral to octahedral [1].

In particular, the acetate group provides the primary basic structural motif for constructing coordination complexes. Its coordination chemistry has been in-depth studied, mainly acting as a bridging ligand, showing a wide range of coordination modes such as: μ_2 -1,1-OAc [2], μ_2 -1,3-OAc [3], μ_3 -1,1,3-OAc [4]. Cu(II) acetates have been widely used not only as a starting reagent but also in the synthesis of coordination compounds [5] and exhibiting different arrays [6]. The most common array when Cu(II) acetates are in presence of monodentate *N*-donor ligands is the formation of dimeric paddle-wheels species with the auxiliary ligands occupying the apical sites [7].

There are less reported cases in which the bridging acetate units exhibit a μ_2 -1,1-OAc coordination mode [8]. This tendency is mainly governed by additional factors as: solvent, pH, temperature or concentration [9]. Among them, solvent is one of the key factors concerning its polarity, boiling point, dielectric constant or van der Waals radii, which have a determining effect in the synthesis process [10]. The final product can be modified if solvent acts as ligand [11], as guest [12], as both [13] or simply directs the final structure [14]. For this reason, in most of cases, the solvent of the reaction defines the molecular array and as a result, many efforts have been devoted to research the role of the solvent in the assemblies of coordination compounds [15].

Numerous dimeric Cu(II) compounds formulated as $[\text{Cu}^{\text{II}} \text{X}_2\text{L}_2]$ (X = acetate or derivatives and L = pyridine and derivatives) have been reported [16]. Among these auxiliary ligands, isonicotinamide (Isn) outstands being an antitubercular, antipyretic, fibrinolytic and antibacterial medicinal agent [17]. It is also available as a drug candidate to prevent and/or release diabetes by protecting β -cells from damage and death [18]. It is worthwhile to mention that Isn has a higher pKa value (10.61) than other pyridine derivative ligands. In addition, it is a valuable directing motif for its role as a mainstone in the resulting architecture, these is due to its characteristic amide-amide pattern and its potential for constructing supramolecular 1D chains [19].

In the field of supramolecular chemistry, suitable directing motifs (synthons), either belonging to *N*-aromatic donor or carboxylic ligands have been thoroughly studied. In the crystalline inception, a hierarchical assembly of the interactions present in the system will determine the ordering of the final structure. The fact that carboxylic acids and amides are empowered to form robust architectures via O-H \cdots O and N-H \cdots O [20] make them widely used motifs and their combination well suited for crystal engineering, although this mechanism is still not well-understood [21].

Our group has already performed the synthesis of monomeric and dimeric species [22] containing Cu(II) and 1,3-benzodioxole-5-carboxylic acid (piperonylic acid, HPip). In this sense, the use of $\text{Cu}(\text{OAc})_2$ as the building unit and its reaction with four pyridine derivative ligands (dPy = 3-phenylpyridine (3-ppy), 2-benzylpyridine (2-bzpy), 4-benzylpyridine (4-bzpy) and 4-acetylpyridine(4-Acpy)) yielded four acetate-based paddle-wheel complexes with the formula $[\text{Cu}(\mu\text{-OAc})_2(\text{dPy})]_2$ [23]. Besides that, the same reaction with 4-ppy resulted in a monomeric compound $[\text{Cu}(\text{OAc})_2(4\text{-ppy})_2(\text{H}_2\text{O})_{1.5}]$ [24]. Recently, we have studied the synthesis of the heteroleptic *core*

[Cu(μ -OAc)(μ -Pip)(MeOH)]₂ (**1**) paddle-wheel compound and its reactions with pyridine and pyrazole derivatives, which resulted in monomeric [Cu(Pip)₂(dPy)₂(H₂O)] and dimeric paddle-wheel [Cu(Pip)₂(dmf)]₂ and [Cu(Pip)₂(dPy)]₂ compounds [25].

As a continuation of this work, in this paper we present the reactivity of **1** [25] with Isn ligand in different solvents, with the finality of study the solvent-dependent formation of a set of compounds (monomers and dimers) and discuss the role of Isn in their supramolecular structures. Reactions performed in methanol (MeOH), *N,N*-dimethylformamide (dmf), water (H₂O), dimethylsulfoxide (dmsO) and acetonitrile (MeCN), yielded dimeric ([Cu(μ -OAc)(OAc)(Isn)₂(solvent)]₂, solvent = MeOH (**2a**), dmf/H₂O (**3**) or H₂O/HPip (**4a**)), paddle-wheel ([Cu(μ -OAc)₂(Isn)]₂·2dmsO(**5**)) and monomeric compounds [Cu(OAc)₂(Isn)₂(HOAc)]·HOAc (**6**). In contrast to the previous results, in all the cases, the two coordinated Pip units are displaced from the heteroleptic *core* and OAc units are maintained units (Scheme 1). All these compounds have been characterized by analytical and spectroscopic techniques and its X-ray crystal structures are solved. Besides, the 2D supramolecular networks of all these compounds are discussed.

Results and discussion

2.1. Synthesis and general characterization

All the reactions have been performed starting from [Cu(μ -OAc)(μ -Pip)(MeOH)]₂ (**1**) precursor, which was previously synthesized in our research group [25], with Isn in different solvents. The synthesis of the three dimeric species with the formula [Cu(μ -OAc)(OAc)(Isn)₂·solvent (solvent = 2MeOH (**2a**), 2dmf/2H₂O (**3**) or 2HPip/4H₂O (**4a**)), was done under reflux conditions for **2a** and **4a**, and at room

temperature (r.t.) for **3**. For compound **4a**, and trying to displace the OAc units, an excess of HPip with additional reaction time was tried. Surprisingly, the HPip has been occluded instead of coordinated. All of them share the same molecular array, but the difference in the occluded solvent molecules morphs its supramolecular nets.

Compound $[\text{Cu}(\mu\text{-OAc})_2(\text{Isn})_2] \cdot 2\text{dmsO}$ (**5**) results to the reaction between **1**, HPip and Isn using dmsO as solvent at r.t.. This compound, different from the three previous ones, exhibited a paddle-wheel structure, with two occluded dmsO molecules. Finally, reaction of **1** with Isn in MeCN as solvent, under reflux conditions, yielded the monomeric specie $[\text{Cu}(\text{OAc})_2(\text{Isn})_2(\text{HOAc})] \cdot \text{HOAc}$ (**6**). It is worthwhile to mention that the pKa of the Isn (10.61) is more basic than the other pyridine derivatives (3-ppy (4.80), 2-bzpy (5.13), 4-bzpy (5.74) and 4-AcPy (3.51)). The different results in the reactions performed between **1** and Isn or between **1** and the mentioned pyridine derivatives, could be promoted by this difference in the pKa value.

Compounds **2a** and **6** have been previously reported by C.B. Aakeröy *et al.* [26], and compound **5** by D. Chisca *et al.* [27] but in all the cases *via* different synthetic method that the described in this paper. Compound **6** was directly isolated and crystallized in the monomeric form without the previous synthesis of the paddle-wheel array. In the case of **5**, the product is also formed in presence of an additional carboxylate moiety (Pip). Herein, the precursor [25] already contained the carboxylate unit and in the same vein, the final product only presents OAc units.

All compounds were characterized by elemental analysis (EA), Attenuated Total Reflectance - Fourier Transformation Infrared Spectroscopy (ATR-FTIR) and single crystal X-ray diffraction. EA of compounds **3**, **5-6** are in accordance with the single crystal X-ray diffraction data. Compounds **2a**, **4a** unavoidably suffer a loss of solvent

molecules after manipulations required for EA (one MeOH (**2a**) and two H₂O molecules(**4a**)) yielding compounds [Cu(μ -OAc)(OAc)(Isn)₂]₂·1.5MeOH (**2b**) and [Cu(OAc)(OAc)(Isn)]₂·2H₂O·2HPip (**4b**).

The ATR-FTIR spectra of compounds **2a-6** display the characteristic carboxylate bands in the range 1591-1568 cm⁻¹ for [$\nu_{as}(\text{COO})$] or 1409-1392 cm⁻¹ for [$\nu_s(\text{COO})$]. The difference between these bands ($\Delta = \nu_{as}(\text{COO}) - \nu_s(\text{COO})$) [28], for compounds **2b-6** is 174, 175, 176, 167 and 196 cm⁻¹, respectively. This difference corresponds to a bidentate bridged (**2b-5**) and a monodentate (**6**) coordination mode of the carboxylate moieties. Also $\nu(\text{O-H})/(\text{N-H})$ from H₂O and Isn (3474-3076 cm⁻¹) or the $\nu(\text{C=O})$ bands from the Isn, HPip (**4b**) or dmf (**3**) molecules appear in the range 1704-1670 cm⁻¹. For compound **5**, some specific bands have been also attributed as $\nu(\text{S=O})$ and $\nu(\text{C-S})$ at 1018 and 706 cm⁻¹, respectively (SI: Fig. S1-S5).

For complex **4a** TG-DTA determination was performed showing the temperature-dependent stepped loss of solvent occluded molecules.

2.2. Crystal structure of compounds **2a-4a**

Compound **2a** was already solved by Aakeröy *et al.* [26] but starting from Cu(OAc)₂·H₂O instead of [Cu(μ -OAc)(μ -Pip)(MeOH)]₂ (**1**) and the structure was solved at different temperature (in this paper at 100K while Aakeröy *et al.* [26] solved at 203K) exhibiting some differences in the supramolecular network (*vide infra*).

The compounds (**2a-4a**) contain four Isn ligands and four OAc units, which form a dimeric array. The OAc units display two different coordination modes: two of them joins the metal ions *via* $\mu_2-1,1$ -OAc bridging mode while the others two are monodentate (Fig.

1). These dimeric architectures are constructed around two Cu(II) metal ions, each one presenting a [CuO₃N₂] core. Both Cu(II) centers exhibit a square pyramidal geometry ($\tau = 0.12$ (**2a**), 0.31 (**3**) and 0.17 (**4a**)) [29]. The basal plane of the square pyramid is composed by one of each different coordinated acetate units (one monodentate and one ditopic bidentate bridged) and the two nitrogen atoms from the Isn ligands while the remaining farthest bridging oxygen atom hold the apical position. Likewise, the Cu...Cu separation within the dimeric unit is in range (3.380-3.449 Å) of few similar compounds [26, 30], and larger than those exhibiting a paddle-wheel structure [7c, 7d]. The coordinated *N*- and *O*-groups are comprised in perpendicular planes. The four pyridil rings exhibit a weak π - π intramolecular interaction at 3.741 Å. There is not many dimeric Cu(II) arrays in which one bridging oxygen has an apical arrangement [31]. Selected distances and angles are shown in Table 1.

2.3. Extended structure of compounds 2a-4

Compounds **2a-4** display the same dimeric array [Cu(μ -OAc)(OAc)(Isn)₂]₂·(solvent) (solvent = 2.5MeOH (**2a**), 2dmf/2H₂O (**3**) or 2HPip/4H₂O (**4**)). These architectures constantly have a 1D expansion derived from the amide-amide pattern (Fig. 2a). The dimeric compositions are tied through the solvent molecules generating two- (**2a** and **3**) and three-dimensional (**4**) supramolecular networks and the different behavior of the solvent molecules constructs different supramolecular architectures (Table 2).

In compound **2a**, as mentioned before, the amide-amide interaction gives an additional 1D expansion and associates dimeric units along the (1 1 1) plane (Table 2). These dimeric arrays are joined by methanol molecules *via* double bridge (amide-

methanol-acetate and *vice versa*) constructing a one-dimensional double chained intermolecular association through the *b* axis. Compared with the previously described in the literature [26], the main difference between both structures is the weakly interacting occluded MeOH molecule, which interacts with the methyl group of a monodentate OAc unit and with the *ortho*-hydrogen atom of a neighbouring Isn ligand (Fig. 2b). In 2a, the furthest MeOH molecule has a weak C-H...O interaction (C2H-H2WB...O6, 136.03°), while in the compound previously solved [26], is not directional enough for being considered a hydrogen bond interaction (C2S-H2SA...O42, 110.50°) (Table 3) [32]. Those associations drive the final 2D supramolecular layers through the *ac* plane (Fig. 3a). The space occupied by these solvent molecules (Fig. 3d) generates an accessible volume of 11.76 Å³ (1.2% of the cell volume). Under air exposure, the one guest MeOH molecule is lost, as indicated by elemental analysis results.

This fluctuation is reasonably understood by the fact that methanol molecules are not a powerful supramolecular synthon and its interactions are weak, so the difference in temperature could be enough for break it. There are reported evidences that supramolecular networks can change depending on the temperature [23b] and this effect is sharper in weaker interactions. Those arising from the amide and the remaining coordinated MeOH molecule don't suffer major changes.

In the supramolecular assembly of compound 3, Isn ligands also play a crucial role stacking dimeric units *via* hydrogen bond interactions through the *b* axis by means of the amide-amide pattern (Table 2). Breaking down this network, Isn molecules have two different interactions; one with an occluded water molecules through the *c* axis and the other, with a double interaction C-H...O and N-H...O with the monodentate acetate (Fig. 2c). All these associations construct the 2D net along the *bc* plane (Fig. 3b). The

space occupied by these solvent molecules (Fig. 3e) generates an accessible volume of 109.17 Å³ (9.6% of the cell volume).

Finally, compound **4a** shows a great number of interactions promoted by occluded molecules (2HPip and 4H₂O). The HPip ligands are entrapped being withheld by two intermolecular hydrogen bond interactions. The carbonylic oxygen atom of the HPip ligand interacts with a bidentate bridging acetate moiety via O-H...O while the protonated oxygen atom interacts with a water molecule. In this sense, the water molecules are the driving force in the supramolecular architecture construction. These four water molecules are divided in two structurally different pairs. Two of them, those with less and weaker hydrogen bond interactions, join the HPip ligands with the waters crux (Fig. 2d). By comparison, the remaining water molecules hold together both water molecules and on top of that, interlink the dimeric arrays through two additional interactions: one with the Isn ligand and one with the monodentate acetate ligand. These set of interactions forms 2D layers along the *ab* plane (Fig. 3c). The space occupied by these solvent molecules (Fig. 3f) generates an accessible volume of 155.38 Å³ (11.8% of the cell volume). All the intermolecular interaction distances and angles for compounds **2a-4a** are provided in Table 2.

2.4. Crystal and extended structure of compound 5

Compound **5** exhibit a dimeric paddle-wheel structure with four bidentate bridged OAc ligands in a *syn-syn* disposition and two Isn units. Each Cu(II) center presents a [CuO₄N] core with a square pyramidal geometry ($\tau = 0.003$) [29] (Table 4). The four OAc are located in the basal plane while the Isn occupies the apical position (Fig. 4a).

Those apical Isn molecules held together the paddle-wheel units through the (1 1 1) direction. In addition, the occluded dmsso molecules not only interacts with the Isn ligand

but also bridges the dimeric arrays along the *b* axis (Table 5). Both interactions form 2D paddle-wheel layers (Fig. 4b). The space occupied by these dmso molecules (Fig. 4c) generates an accessible volume of 198.26 Å³ (25.5% of the cell volume).

2.5. Crystal and extended structure of compound 6

The monomeric array is formed by a [CuO₂N₂] core in which the central Cu(II) ion is surrounded by two OAc, two Isn and one furthest HAcO ligands (Fig. 5a). All this set of ligands design a distorted square-pyramidal geometry ($\tau = 0.31$) [29] around the metal node. The basal plane is formed by the two Isn ligands and two monodentate OAc units while the carbonylic oxygen atom of the HAcO ligand occupies the apical position (Table 6). Both, the fact that axial position belongs from the HAcO ligand (less coordinative than the corresponding deprotonated Lewis base) and the Jahn-teller effect [33], commonly exhibited by Cu(II) d⁹ compounds, favors the weakening of the (Cu-O9) bond and the consequent elongation at the apical site (Fig. 5a). Coordinated HOAc unit presents an intramolecular hydrogen bond interaction with the coordinated OAc (O10-H10O...O3, 2.637(3) Å). As stated before, the effect of the temperature in the crystal structure determination (100K for 6, while Aakeröy *et al.* solved at 203K [26]) is noticeable marked in the intramolecular interaction promoted by the occluded HOAc unit (O51-H51...O31, 2.634 Å, 170.4° in the structure of Aakeröy [26]) while in 6 the values are O10-H10O...O3, 2.637(3) Å, 140.88(7)° (Table 7).

In the extended structure of 6, Isn ligand plays a double role driving the supramolecular network while the occluded HOAc molecule has not a significant role in the formation of the nets. The expansion can be divided through the interaction of Isn with itself and with the two oxygen atoms of the coordinated OAc ligand (Table 8). Isn ligand interacts with one monodentate OAc (Cu-O5) in an alternate manner; either *via* N-

H_{anti} or combining N-H_{anti} with one aromatic C-H_{meta} proton (Fig. 5b). If the hydrogen bond acceptor is the monodentate oxygen atom (Cu-O5) (Fig. 5a), Isn only acts as a single hydrogen bond donor, by contrast, if the acceptor is the non-coordinated oxygen atom of the same monodentate OAc ligand, Isn acts as a double hydrogen bond donor. This double-chained interaction expands the structure through the *c* axis. The amide-amide interaction gives an additional dimensionality through the *a* axis generating 2D layers along the *ac* plane (Fig. 5b). The occluded HOAc unit presents a hydrogen bond interaction with a uncoordinated oxygen atom from the monodentate OAc units. The difference of this interaction (O8-H8A...O4, 2.014 Å, 140.88°) with respect to the structure of Aakeröy *et al.* [26] (O61-H61...O32, 1.823 Å, 173.01°) is also remarkable. These fluctuations in the intra- and intermolecular interactions are higher than the previously reported case for a Cu(II) acetate based structure [23b]. The space occupied by these HOAc molecules (Fig. 5c) generates an accessible volume of 116.49 Å³ hole (4.6 % of the cell volume).

2.7. Hirshfeld Surface Analysis

Hirshfeld surfaces analyses of all the structures have been performed with CrystalExplorer 2.1 [34]. It is a powerful graphical tool for evaluate the interactions present in crystal structures, aiming for the better understanding of the intermolecular forces present in these systems and for comparison between them. The d_{norm} surface mapping shows red spots on the main interactive points of the surface generated and the main interactions outline in the 2D fingerprint plots. These plots show all of the intermolecular interactions (including hydrogen). Additional Hirshfeld surface mappings of the occluded solvent molecules are illustrated in S.I.: Fig.S6-S7. All these surfaces have been calculated at an isovalue of 0.5 e au⁻³.

From all this set of compounds, the d_{norm} surface mapping shows two red marked spots in each amidic group of the Isn ligand. The 2D fingerprint plots show two sharp peaks related to the complementary Isn...Isn interaction (Fig. 6). This association is maintained in all the surfaces of the complexes and overcomes from the rest. In compounds **3-6** the OAc units interacts with the N-H_{anti} proton of the amidic moiety and can be identified in the 2D fingerprint plot, appearing with the amide...amide interaction. Different from the previous, in **2a** the MeOH occluded molecules interacts with the OAc avoiding its interaction with the mentioned N-H_{anti}, and for this reason the interaction could not be identified. It can be noted that dimeric units (**2a-4a**) have a spatial disposition in which aromatic pyridil rings are placed at a 4.8 Å distance. Concretely, compound **3**, in which monodentate acetates generates less interactions, the region corresponding to the oxygen atom interactions is reduced and this interaction is exposed as an small peak (Fig. 6.b).

2.8. TG-DTA analysis

Simultaneous TG-DTA determinations were carried out to evaluate the thermal stability of compound **3a**. The measurement was performed using 67.1 mg of sample. The thermogravimetric decomposition curve shows a four-staged mass loss (Fig. 7). A first minor step attributed to the loss of two water molecules occurs between 37 and 75 °C (weight loss exp. 2.5%, calc. 2.9%). The second weight loss occurs between 75 and 142 °C and can be assigned to loss of two water and one HPip molecules (weight loss exp. 16.4%, calc. 16.0 %). The last weight loss before decomposition occurs between 142 and 211 °C which can be attributed to the loss of a second HPip molecule (weight loss exp. 13.3%, calc. 13.2%). From this temperature, the compound continues its decomposition ending at 275 °C.

3. Conclusion

In this paper, we present the reaction of $[\text{Cu}(\mu\text{-OAc})(\mu\text{-Pip})(\text{MeOH})_2]$ (**1**) with Isn in different solvents which promotes the formation of different structural arrays by the different coordination mode of the OAc units. The resulting five compounds exhibit dimeric (**2a-4a**), paddle-wheel (**5**) and monomeric (**6**) structures. In all these compounds, the Pip units are displaced from **1** while OAc units remains coordinated. This behavior is different in comparison with the previous work, in which the Pip units remained coordinated and the OAc units were displaced resulting in monomeric and paddle-wheel compounds [22b]. It could be noted that the formation of the molecular array is determined by the Isn ligand. The amide group of the Isn ligand, a powerful supramolecular synthon, associates the complexes *via* hydrogen bond interactions forming 1D linear chains, which solvent occluded molecules expand to 2D (**2a**, **3**, **5** and **6**) or 3D (**4a**) nets. Regardless of the spatial distribution and connectivity of the OAc ligands, the role of the Isn ligand as supramolecular 1D building unit is maintained as supported by the Hirshfeld structural analysis.

4. Experimental Section

4.1 Materials and methods

Cu(II) acetate monohydrate ($\text{Cu}(\text{OAc})_2 \cdot \text{H}_2\text{O}$), 1,3-benzodioxole-5-carboxylic acid (piperonylic acid, HPip), acetic acid (HAcO) and isonicotinamide (Isna) ligands; methanol (MeOH), *N,N*-dimethylformamide (dmf), dimethylsulfoxide (dmsO), acetonitrile (MeCN) and water were used as solvents. All of them were purchased from Sigma-Aldrich and used without further purification. Elemental analysis (C, H, N) were carried out on a Thermo Scientific Flash 2000 CHNS Analyser. The ATR-FTIR spectra were recorded on a Perkin Elmer spectrometer, equipped with a universal attenuated total

reflectance (ATR) accessory with diamond window in the range 4000-500 cm^{-1} . Simultaneous TG-DTA determination of compound **4a** was carried out in a Netzsch STA 409 instrument in an aluminium oxide (Al_2O_3) crucible and heating at $5^\circ\text{C}\cdot\text{min}^{-1}$ from 25 to 450°C , under a nitrogen atmosphere with a flow rate of 80 mL/min. Al_2O_3 powder (Perkin-Elmer 0419-0197) was used as Standard. The $[\text{Cu}(\mu\text{-OAc})(\mu\text{-Pip})(\text{MeOH})_2]$ (**1**) precursor was previously synthesized in our research group [25].

4.2 Synthesis of compounds **2a-6**

4.2.1. $[\text{Cu}(\mu\text{-OAc})(\text{OAc})(\text{Isn})_2]_2\cdot 2.5\text{MeOH}$ (**2a**)

A MeOH solution (25 mL) of **1** (200 mg, 0.313 mmol) was added dropwise to a MeOH solution (15 mL) of Isn (76.5 mg, 0.626 mmol). Addition of 2 mL of HAcO for clear solution and stirred vigorously under reflux conditions for 15 h. Mother liquors were evaporated until dark blue solid precipitated. Blue powder was filtered and washed with 10mL of cold methanol and dried under vacuum. Suitable crystals were obtained after slow evaporation of the mother liquors on air for three days. The stoichiometry of this compound was definitely established after resolution of their X-ray crystal structure. However, one occluded MeOH solvent molecule is withdrawn from the structure after manipulation required for preparing the sample for EA yielding $[\text{Cu}(\mu\text{-OAc})(\text{OAc})(\text{Isn})_2]_2\cdot 1.5\text{MeOH}$ (**2b**).

2b. Yield: 123 mg (86%). Elem. Anal. Calc. for $\text{C}_{33.5}\text{H}_{42}\text{Cu}_2\text{N}_8\text{O}_{13.5}$ (915.85 g/mol): C 44.71; H 4.88; N 12.45. Found: C 44.95; H 4.57; N 12.28%. ATR-FTIR (wavenumber, cm^{-1}): 3314(m) $[\nu(\text{O-H})]_{\text{MeOH}}$, 3157(m) $[\nu(\text{N-H})]$, 3076(m) $[\nu(\text{N-H})]$, 3063(w) $[\nu_{\text{ar}}(\text{C-H})]$, 2938(w) $[\nu_{\text{al}}(\text{C-H})]$, 2809(m), 1693(s) $[\nu(\text{C=O})]_{\text{Isn}}$, 1638(w), 1614(m), 1593(m), 1568(m) $[\nu_{\text{as}}(\text{COO})]$, 1556(m) $[\nu(\text{C=C/C=N})]$, 1505(w), 1454(w), 1442(w), 1418(m) $[\delta(\text{C=C/C=N})]$, 1394(s) $[\nu_{\text{s}}(\text{COO})]$, 1380(s), 1335(m), 1231(m), 1221(m), 1156(w),

1126(w), 1104(w), 1066(w), 1046(w), 1018(m) [$\delta_{ip}(\text{C-H})$], 930(w), 882(w), 860(w), 800(w), 770(w) [$\delta_{oop}(\text{C-H})$], 716(w), 676(m), 650(m), 620(s) [$\delta(\text{O=CN})$], 541(m), 504(m).

4.2.2. $[\text{Cu}(\mu\text{-OAc})(\text{OAc})(\text{Isn})_2]_2 \cdot 2\text{dmf} \cdot 2\text{H}_2\text{O}$ (**3**)

A dmf solution (10 mL) of **1** (100 mg, 0.156 mmol) was added dropwise to a dmf solution (10 mL) of Isn (227 mg, 0.313 mmol) with 1 mL of H₂O and 2 mL of HAcO and was stirred vigorously for 5 hours. The resulting dark blue solution was evaporated until half of the volume and cooled down. After one day a dark blue solid precipitated. Powder was filtered and washed with 10 mL of cold methanol and dried under vacuum. Suitable crystals were obtained by slow evaporation of the solid recrystallized in dmf for 4 days. Compound **3** was also obtained via recrystallization of **2a** in dmf.

Yield: 70.3 mg (81%). Elem. Anal. Calc. for C₃₈H₅₄Cu₂N₁₀O₂₀ (1033.98 g/mol): C 44.14; H 5.26, N 12.76. Found: C 44.38; H 4.83; N 12.54%. ATR-FTIR (wavenumber, cm⁻¹): 3474(w) [$\nu(\text{O-H})_{\text{water}}$], 3380(m) [$\nu(\text{O-H})_{\text{water}}$], 3327(m) [$\nu(\text{O-H})_{\text{water}}$], 3161(m) [$\nu(\text{N-H})$], 3108(m), 3080(m) [$\nu(\text{N-H})$], 3063(m) [$\nu_{\text{ar}}(\text{C-H})_{\text{Isn}}$], 2961(w) [$\nu_{\text{al}}(\text{C-H})_{\text{DMF}}$], 2927(w) [$\nu_{\text{al}}(\text{C-H})_{\text{OAc}}$], 2884(w), 1704(m) [$\nu(\text{C=O})_{\text{Isn}}$], 1660(m) [$\nu(\text{C=O})_{\text{DMF}}$], 1632(w) [$\nu(\text{C=O})_{\text{DMF}}$], 1614(m), 1596(m), 1576(m) [$\nu_{\text{as}}(\text{COO})$], 1554(m) [$\nu(\text{C=C/C=N})$], 1508(w), 1495(w), 1422(m) [$\delta(\text{C=C/C=N})$], 1401(s) [$\nu_{\text{s}}(\text{COO})$], 1377(s), 1343(m), 1324(s), 1256(w), 1231(m), 1226(m), 1154(w), 1122(w), 1100(m), 1067(m), 1047(w), 1028(m) [$\delta_{ip}(\text{C-H})$], 984(w), 927(w), 865(m), 849(w), 792(m) [$\delta_{oop}(\text{C-H})$], 768(w), 738(w), 673(m), 666(m), 647(s) [$\delta(\text{O=CN})$], 620(m), 555(m).

4.2.3. $[\text{Cu}(\mu\text{-OAc})(\text{OAc})(\text{Isn})_2]_2 \cdot 2\text{HPip} \cdot 4\text{H}_2\text{O}$ (**4a**)

A MeOH solution (25 mL) of **1** (100 mg, 0.156 mmol) was added dropwise to a MeOH solution (15 mL) of Isn (227 mg, 0.313 mmol) with HPip (26.0 mg, 0.156 mmol), 1 mL

of H₂O and 2 mL of HOAc. The resulting clear blue solution was stirred under reflux conditions for a week. Mother liquors were evaporated until half of the volume and kept on air. The resulting blue powder was filtered off, washed with 10 mL of cold methanol and dried under vacuum. Suitable crystals were obtained by slow evaporation of mother liquors for 18 days. The stoichiometry of this compound was definitely established after resolution of their X-ray crystal structure. However, two occluded water solvent molecules are withdrawn from the structure after manipulation required for preparing the sample for EA yielding [Cu(μ -OAc)(OAc)(Isn)₂]₂·2HPip·2H₂O (**4b**). This result is supported by the TG/DTA analysis (Fig. 7).

4b. Yield: 149.01 mg (78%). Elem. Anal. Calc. for C₄₈ H₅₂ Cu₂ N₈ O₂₂ (1220.06 g/mol): C 47.25; H 4.30; N 9.18. Found: C 46.91; H 4.01; N 9.03%. ATR-FTIR (wavenumber, cm⁻¹): 3414(m), 3373(m) [v(O-H)]_{water}, 3325(m) [v(O-H)]_{HPip}, 3168(s) [v(N-H)], 3117(m), 3087(m) [v(N-H)], 3018(w) [v_{ar}(C-H)], 2906(w) [v_{al}(C-H)], 2838(w) [v_{al}(C-H)], 2788(w)-2482(w) [overlapping C-H bands from HPip], 1702(m) [v(C=O)]_{Isn}, 1668(m) [v(COO)]_{HPip}, 1636(w), 1616(w), 1606(w), 1568(s) [v_{as}(COO)], 1556(m) [v(C=C/C=N)], 1504(m), 1471(w), 1444(m) [δ (C=C/C=N)]_{HPip}, 1421(m) [δ (C=C/C=N)]_{Isn}, 1392(s) [v_s(COO)], 1348(m), 1340(m), 1256(s), 1234(m), 1221(m), 1162(m) [v(C-O-C)], 1115(m), 1068(m), 1030(m) [δ _{ip}(C-H)], 974(w), 929(m), 913(m), 884(w), 858(m), 811(w), 786(w), 764(s) [δ _{oop}(C-H)], 718(w), 679(m), 647(s) [δ (O=CN)], 621(m), 579(m).

4.2.4. [Cu(μ -OAc)₂(Isn)]₂·dmsO (**5**)

A dmsO solution (10 mL) of **1** (100 mg, 0.156 mmol) with 1mL of HAcO was added dropwise to a dmsO solution (10 mL) of Isn (187.5 mg, 0.154 mmol) and stirred at r.t. A green precipitate appeared after 1h. Powder was filtered off and washed with 10 mL of cold methanol and dried under vacuum. Suitable crystals were obtained by

recrystallization of the powder in dmsO for six days. Compound **5** was also obtained *via* recrystallization of **2a** in dmsO.

Yield: 265.8 mg (45%). Elem. Anal. Calc. for C₂₄H₃₆Cu₂N₄O₁₂S₂ (763.77 g/mol): C 37.74; H 4.75; N 7.34; S 8.40. Found: C 37.68; H 4.77; N 7.25; S 8.19%. ATR-FTIR (wavenumber, cm⁻¹): 3290(m), 3150(m) [ν(N-H)], 3099(w) [ν(N-H)], 3013(w) [ν_{ar}(C-H)], 2998(w) [ν_{al}(C-H)], 2917(w) [ν_{al}(C-H)], 2598(w), 1670(m) [ν(C=O)]_{Isn}, 1611(s), 1576(m) [ν_{as}(COO)], 1556(s) [ν(C=C/C=N)], 1542(m), 1504(m), 1428(m) [δ(C=C/C=N)], 1409(s) [ν_s(COO)], 1341(m), 1307(m), 1220(m), 1153(w), 1122(w), 1101(w), 1069(w), 1047(m) [δ_{ip}(C-H)], 1018(s) [ν(S=O)], 958(m), 940(w), 900(w), 859(m), 816(w), 766(w), 706(m) [ν(C=S)], 678(s) [δ_{oop}(C-H)], 660(s), 641(s), 626(s) [δ(O=CN)]

4.2.5. [Cu(OAc)₂(Isn)₂(HOAc)]·HOAc (**6**)

A MeCN solution (25 mL) of **1** (100 mg, 0.156 mmol) with 1 mL of HAcO was added dropwise to a MeCN solution (20 mL) of Isn (187 mg, 0.154 mmol). Reaction was stirred under reflux conditions for 2 h until a pale blue solid appeared. Powder was filtered off, washed with 10 mL of cold methanol and dried under vacuum. Suitable crystals were obtained by slow evaporation of mother liquors for 5 days. Compound **6** was also obtained *via* recrystallization of **2a** in MeCN.

Yield: 138.2 mg (81%). Elem. Anal. Calc. for C₂₀H₂₆CuN₄O₁₀ (545.99 g/mol): C 44.00; H 4.80; N 10.26. Elem. Anal. Found: C 43.78; H 4.72; N 10.05%. ATR-FTIR (wavenumber, cm⁻¹): 3570(m), 3504(m), 3413(m) [ν(O-H)], 3311(br.) [ν(O-H)], 3175(m) [ν(N-H)], 3107(m) [ν(N-H)], 3067(m) [ν_{ar}(C-H)], 2930(w) [ν_{al}(C-H)], 2852(w), 2809(w), 2656(w), 1692(s) [ν(C=O)]_{Isn}, 1613(s), 1591(s) [ν_{as}(COO)], 1554(s) [ν(C=C/C=N)]_{Isn}, 1415(m) [δ(C=C/C=N)], 1395(s) [ν_s(COO)], 1375(s), 1316(s), 1228(m), 1222(m),

1151(m), 1126(m), 1103(w), 1065(m) [$\delta_{ip}(\text{C-H})$], 1026(m), 1004(w), 967(w), 926(w), 883(w), 856(m), 780(m) [$\delta_{oop}(\text{C-H})$], 761(m), 709(w), 677(s), 647(s), 623(s) [$\delta(\text{O=CN})$], 523(s).

4.3 X-ray single crystal diffraction method

For compounds **2a-6** a blue prism-like specimen was used for the X-ray crystallographic analysis. The X-ray intensity data were measured on a D8 Venture system equipped with a multilayer mono-chromate and a Mo microfocus ($\lambda = 0.71073 \text{ \AA}$). For all compounds, the frames were integrated with the Bruker SAINT Software package using a narrow-frame algorithm. For **2a**, the integration of the data using a triclinic unit cell yielded a total of 53538 reflections to a maxim θ angle of 30.55° (0.70 \AA resolution), of which 6222 were independent (average redundancy 8.605, completeness = 99.4%), $R_{\text{int}} = 3.20\%$, $R_{\text{sig}} = 2.04\%$ and 5520 (88.72%) were greater than $2\sigma(F^2)$. The calculated minimum and maximum transmission coefficients (based on crystal size) are 0.6892 and 0.7461. For **3**, the integration of the data using a triclinic unit cell yielded a total of 22855 reflections to a maxim θ angle of 27.64° (0.77 \AA resolution), of which 5157 were independent (average redundancy 4.432, completeness = 97.9%), $R_{\text{int}} = 7.29\%$, $R_{\text{sig}} = 5.64\%$ and 3986 (77.29%) were greater than $2\sigma(F^2)$. The calculated minimum and maximum transmission coefficients (based on crystal size) are 0.6689 and 0.7456. For **4a**, the integration of the data using a triclinic unit cell yielded a total of 73301 reflections to a maxim θ angle of 30.57° (0.70 \AA resolution), of which 8119 were independent (average redundancy 9.028, completeness = 99.7%), $R_{\text{int}} = 7.51\%$, $R_{\text{sig}} = 4.69\%$ and 6205 (76.43%) were greater than $2\sigma(F^2)$. The calculated minimum and maximum transmission coefficients (based on crystal size) are 0.7160 and 0.7461. For **5**, the integration of the data using a triclinic unit

cell yielded a total of 45152 reflections to a maximum θ angle of 30.55° (0.70 \AA resolution), of which 4755 were independent (average redundancy 9.496, completeness = 99.6%), $R_{\text{int}} = 2.36\%$, $R_{\text{sig}} = 1.30\%$ and 4510 (94.85%) were greater than $2\sigma(F^2)$. The calculated minimum and maximum transmission coefficients (based on crystal size) are 0.6570 and 0.7461. For **6**, the integration of the data using a monoclinic unit cell yielded a total of 34869 reflections to a maximum θ angle of 26.42° (0.80 \AA resolution), of which 5149 were independent (average redundancy 6.772, completeness = 99.8%), $R_{\text{int}} = 8.42\%$, $R_{\text{sig}} = 4.46\%$ and 3790 (73.61%) were greater than $2\sigma(F^2)$. The calculated minimum and maximum transmission coefficients (based on crystal size) are 0.6933 and 0.7454.

The structures were solved using the Bruker SHELXTL Software, package and refined using SHELX (version-2018/3) [35]. For **2a**, the final anisotropic full-matrix least-squares refinement on F^2 with 280 variables converged at $R1 = 2.92\%$, for the observed data and $wR2 = 7.75\%$ for all data. For **3**, the final anisotropic full-matrix least-squares refinement on F^2 with 309 variables converged at $R1 = 4.19\%$, for the observed data and $wR2 = 11.18\%$ for all data. For **4a**, the final anisotropic full-matrix least-squares refinement on F^2 with 390 variables converged at $R1 = 4.00\%$, for the observed data and $wR2 = 8.49\%$ for all data. For **5**, the final anisotropic full-matrix least-squares refinement on F^2 with 203 variables converged at $R1 = 2.07\%$, for the observed data and $wR2 = 5.32\%$ for all data. For **6**, the final anisotropic full-matrix least-squares refinement on F^2 with 319 variables converged at $R1 = 3.79\%$, for the observed data and $wR2 = 8.78\%$ for all data.

For **2a-6**, the final cell constants and volume, are based upon the refinement of the XYZ-centroids of reflections above $20 \sigma(I)$. Data were corrected for absorption effects using the multi-scan method (SADABS). Crystal data and relevant details of structure refinement for compounds **2a-6**, are reported in **Tables S1-S2**. Molecular graphics were

generated with the program Mercury 3.6 [36] Color codes for all molecular graphics: blue (Cu), light blue (N), red (O), grey (C), white (H). Crystal structure and molecular geometry is available in CIF format: CCDC 1905990-1905994 (**2a-6**).

Conflicts of interest

The are no conflicts to declare

Acknowledgements

This work was financed by CB615921 project, the Spanish National Plan of Research MAT2015-65756R, and 2017SGR1687 project from the Generalitat de Catalunya. F. S. acknowledges the PIF pre-doctoral fellowship from the Universitat Autònoma de Barcelona.

.

Appendix A. Supplementary data

Supplementary data to this article can be found on line at [XXXXXXXXXXXX](#).

References

- [1] F.P.W. Agterberg, H.A.J. Kluit, W.L. Driessen, H.Oevering, W. Buijs, M.T. Lakin, A.L. Spek, J. Reedijk, *Inorg. Chem.* 36 (1997) 4321-4328.
- [2] J. E. Barker, Y. Liu, G. T. Yee, W.-Z. Chen, G. Wang, V. M. Rivera and T. Ren, *Inorg. Chem.* 45 (2006) 7973–7980.
- [3] H.-M. Berends, A.-M. Manke, C. Nather, F. Tuzcek and P. Kurz, *Dalton Trans.* 41 (2012) 6215–6224.
- [4] S. K. Langley, B. Moubaraki and K. S. Murray, *Dalton Trans.* 39 (2010) 5066–5069.
- [5] M. Swadzba-Kwasny, L. Chancelier, S. Ng, H. G. Manyar, C. Hardacre and P. Nockemann, *Dalton Trans.* 41 (2012) 219–227.
- [6] a) I. Y. Ahmed, A. L. Abu-Hijleh, *Inorg. Chim. Acta* 61 (1982) 241-246.
b) P. Sharrock, M. Melník, *Can. J. Chem.* 63 (1985) 52-56.
- [7] a) I. Dasna, S. Golhen, L. Ouahab, O. Peña, N. Daro, J-P. Sutter, *New J. Chem.* 24 (2000) 903-906;
b) S. Youngme, A. Cheanisirisomboon, C. Danvirutai, C. Pakawatchai, N. Chaichit, C. Engkagul, G.A. van Albada, J. Sánchez-Costa, J. Reedijk, *Polyhedron*, 27 (2008) 1875;
c) M. Barquín, M. J. G. Garmendia, L. Larrínaga, E. Pinilla, J. M. Seco, M. R. Torres, *J. Coord. Chem.*, 63 (2010), 1652-1665;
d) M. Barquín, N. Cocera, M. J. G. Garmendia, L. Larrínaga, E. Pinilla, M. R. Torres, *J. Coord. Chem.*, 63 (2010), 2247-2260.

- [8] a) V. K. Bhardwaj, N. Aliaga-Alcalde, M. Corbella and G. Hundal, *Inorg. Chim. Acta*, 363 (2010) 97–106.
- b) B. Sarkar, M. G.B. Drew, M. Estrader, C. Díaz, A. Ghosh, *Polyhedron* 27 (2008) 2625-2633;
- c) V. T. Panushkin, T. E. Apenysheva, V. I. Sokol, V. S. Sergienko, K. S. Pushkareva, S. N. Bolotin, F. A. Kolokolov, E. V. Gromachevskaya, A. A. Borodavko, T. P. Kosulina, *Russ. J. Coord. Chem* 33 (2007) 674-679.
- [9] a) C. P. Li , J. M. Wu and M. Du , *Chem. Eur. J.* 18 (2012) 12437 -12445;
- b) S. B. Li , H. Y. Ma , H. J. Pang and L. Zhang, *Cryst. Growth Des.* 14 (2014) 4450 -4460;
- c) L. Y. Du , W. J. Shi , L. Hou , Y. Y. Wang , Q. Z. Shi and Z. H. Zhu, *Inorg. Chem.* 52 (2013) 14018 -14027;
- d) S. J. Yang , J. H. Cho , K. Lee , T. Kim and C. R. Park, *Chem. Mater.* 22 (2010) 6138 -6145.
- [10] a) Y. W. Li , D. C. Li , J. Xu , H. G. Hao , S. N. Wang , J. M. Dou , T. L. Hu and X. H. Bu, *Dalton Trans.* 43 (2014) 15708 -15712;
- b) W. W. Dong , D. S. Li , J. Zhao , L. F. Ma , Y. P. Wu and Y. P. Duan, *CrystEngComm* (2013) 5412 -5416;
- c) X. R. Hao , X. L. Wang , K. Z. Shao , G. S. Yang , Z. M. Su and G. Yuan, *CrystEngComm* 14 (2012) 5596 -5603.

- [11] X. Y. Liu , P. P. Cen , H. Li , H. S. Ke , S. Zhang , Q. Wei , G. Xie , S. P. Chen and S. L. Gao, *Inorg. Chem.* 53 (2014) 8088 -8097.
- [12] T. Wang , C. L. Zhang , Z. M. Ju and H. G. Zheng, *Dalton Trans.* 44 (2015) 6926 - 6935.
- [13] S. C. Chen , Z. H. Zhang , K. L. Huang , Q. Chen , M. Y. He , A. J. Cui , C. Li , Q. Liu and M. Du, *Cryst. Growth Des.* 8 (2008) 3437 -3445.
- [14] J. Li , G. P. Yang , L. Hou , L. Cui , Y. P. Li , Y. Y. Wang and Q. Z. Shi, *Dalton Trans.* 42 (2013) 13590 -13598.
- [15] a) P. V. Bernhardt, H. Font, C. Gallego, M. Martínez, C. Rodríguez, *Inorg. Chem.* 51 (2012) 12372-12379;
- b) J. Zhao, H.-Y. Lin, G.-C. Liu, X. Wang, X.-L. Wang, *Inorg. Chim. Acta* 464 (2017) 114-118;
- c) C.-H. Ge, X.-D. Zhang, W. Guan, Q.-T. Liu, *J. Chem. Cryst.* 36 (2006) 459-464;
- d) M. Baskin, N. Fridman, M. Kosa, G. Maayan, *Dalton Trans.* 46 (2017) 15330-15339.
- [16] a) L. C. Porter, M. H. Dickman, R. J. Doedens, *Inorg. Chem.* 25 (1986) 678-684;
- b) Cambridge Structural Database (CSD) (Version 5.37) (2016).
- [17] A. Ataç, Ş. Yurdakul and S. Ide, *J. Mol. Struct.* 783 (2006) 79–87.
- [18] M. Fukaya, Y. Tamura, Y. Chiba, T. Tanioka, J. Mao, Y. Inoue, M. Yamada, C. Waeber, Y. Ido-Kitamura, T. Kitamura and M. Kaneki, *Biochem. Biophys. Res. Commun.* 442 (2013) 92–98.
- [19] a) J. Moncol, M. Mudra, P. Lönnecke, M. Hewitt, M. Valko, H. Morris, J. Svorec,

- M. Melnik, M. Mazur, M. Koman, *Inorg. Chim. Acta* 360 (2007) 3213-3225;
- b) P. Segl'a, V. Kuchtanin, M. Tatarko, J. Švorec, J. Moncol, M. Valko, *Chem. Pap.* 72 (2018) 863-876;
- c) M. Arici, O. Z. Yeşilel, E. Acar, N. Dege, *Polyhedron* 127 (2017) 293-301;
- d) E. Sayin, G. S. Kürkcüoğlu, O. Z. Yeşilel, T. Hökelek, *J. Mol. Struct.* 1096 (2015) 84-93.
- [20] B. R. Bhogala, P. K. Thallapally and A. Nangia, *Cryst. Growth Des.* 4 (2004) 215–218.
- [21] C. P. Li and M. Du, *Chem. Commun.* 47 (2011) 5958 -5972.
- [22] a) J. Soldevila-Sanmartín, J.A. Ayllón, T. Calvet, M. Font-Bardía, J. Pons, *Polyhedron* 126 (2017) 184-194;
- b) F. Sánchez-Férez, J. Soldevila-Sanmartín, J. A. Ayllón, T. Calvet, M. Font-Bardía, J. Pons, *Polyhedron* 164 (2019) 64-73.
- [23] a) M. Guerrero, J.A. Ayllón, T. Calvet, M. Font-Bardía, J. Pons, *Polyhedron* 134 (2017) 107-113;
- b) J. Soldevila-Sanmartín, M. Sanchez-Sala, T. Calvet, M. Font-Bardía, , J.A. Ayllón, J. Pons, *J. Mol. Struct.* 1171 (2018) 808-814.

- [24] J. Soldevila-Sanmartín, J. A. Ayllón, T. Calvet, M. Font-Bardia, J. Pons, *Polyhedron* 135 (2017) 36-40.
- [25] a) J. Soldevila-Sanmartín, J.A. Ayllón, T. Calvet, M. Font-Bardía, C. Domingo, J. Pons, *Inorg. Chem. Commun.* 71 (2016) 90-93;
b) F. Sánchez-Férez, M. Guerrero, J. A. Ayllón, T. Calvet, M. Font-Bardia, J. G. Planas, J. Pons, *Inorg. Chim. Acta* 487 (2019) 150-157.
- [26] C.B. Aakeröy, A. M. Beatty, J. Desper, M. O'Shea, J. Valdés-Martínez, *Dalton Trans.* (2003) 3956-3962.
- [27] D. Chisca, E. Coropceanu, O. Petuhov, L. Croitor, *Chem. J. Mold.* 10 (2015) 33-39.
- [28] K. Nakamoto, *Infrared and Raman Spectra of Inorganic and Coordination Compounds. Applications in Coordination, Organometallic, and Bioinorganic Chemistry*, sixth ed. Wiley Interscience, New York, USA, 2009.
- [29] A. W. Addison, T.N. Rao, J. Chem. Soc., *Dalton Trans.* 1 (1984) 1349-1356.
- [30] a) B. Kozlevčar, I. Leban, I. Turel, P. Šegedin, M. Petrič, F. Pohleven, A. J. P. White, D. J. Williams, J. Sieler, *Polyhedron* 18 (1999) 755-762;
b) M. A. Pauly, E. M. Erwin, D. R. Powell, G. T. Rowe, L. Yang, *Polyhedron* 102 (2015) 722-734.
- [31] a) J. Pasán, J. Sanchiz, C. Ruiz-Pérez, F. Lloret, M. Julve, *New J. Chem.* 27 (2003) 1557-1562;
b) R. Baldomá, M. Monfort, J. Ribas, X. Solans, M. A. Maestro, *Inorg. Chem.* 45 (2006) 8144-8155;

c)R. Bikas, P. Aleshkevych, H. Hosseini-Monfared, J. Sanchiz, R. Szymczak, T. Lis,
Dalton Trans. 44 (2015) 1782-1789.

[32] T. Steiner, *Angew. Chem. Int. Ed.* 41 (2002) 48-76.

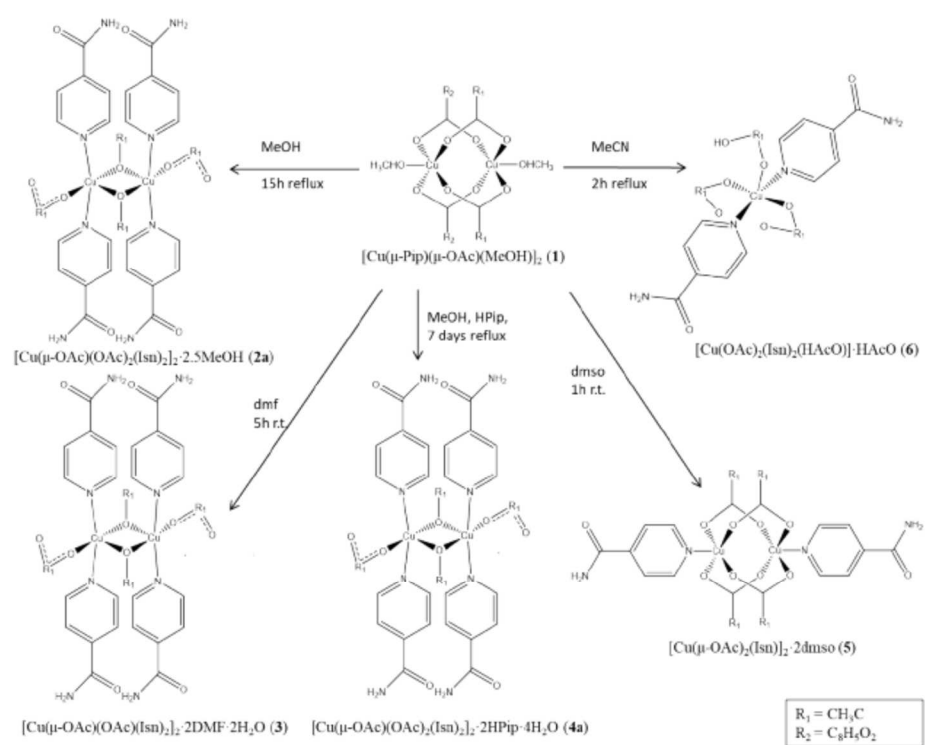
[33] L. R. Falvello *J. Chem. Soc., Dalton Trans.* (1997) 4463-4476.

[34] S. K. Wolff, D. J. Grimwood, J. J. McKinnon, D. Jayatilaka and M. A. Spackman,
CrystalExplorer, version 2.1; University of Western, Australia : Crawley, Australia,
(2007).

[35] G. M. Sheldrick, *Acta Crystallogr. Sect. A Found. Crystallogr.* 64 (2007) 112-122.

[36] (a) C.F. Macrae, P. R. Edgington, P. McCabe, E. Pidcock, G. Shields, R. Taylor,
M. Towler, J.J. van de Streek, *Appl. Crystallogr.* 39 (2006) 453-457;

(b) C.F. Macrae, I.J. Bruno, J.A. Chisholm, P.R. Edgington, P. McCabe, E. Pidcock, I.
Rodriguez-Monge, R. Taylor, M. Towler, J. van de Streek, P.A.J. Wood, *Appl.*
Crystallogr. 41 (2008) 466-470.



Scheme 1. Schematic synthesis of compounds 2a-6.

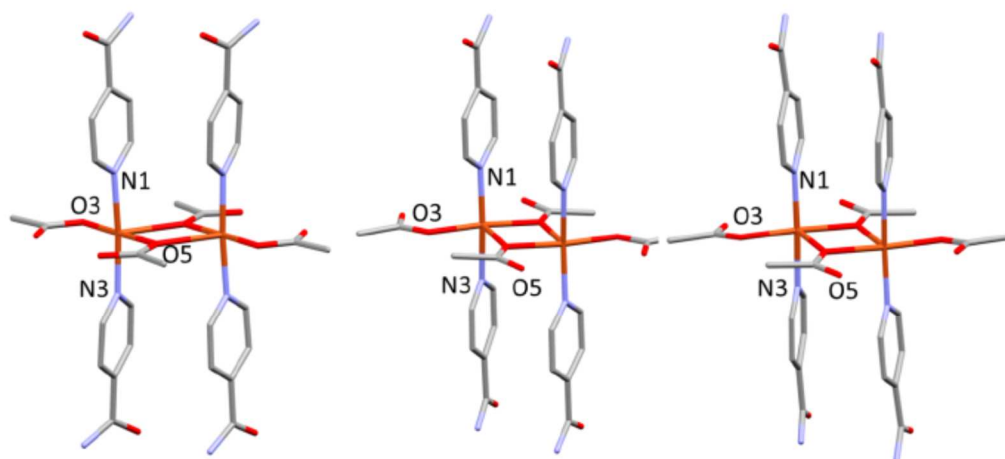


Figure 1. Molecular structure of the compounds **2a-4a**, respectively. Hydrogen atoms are omitted for clarity.

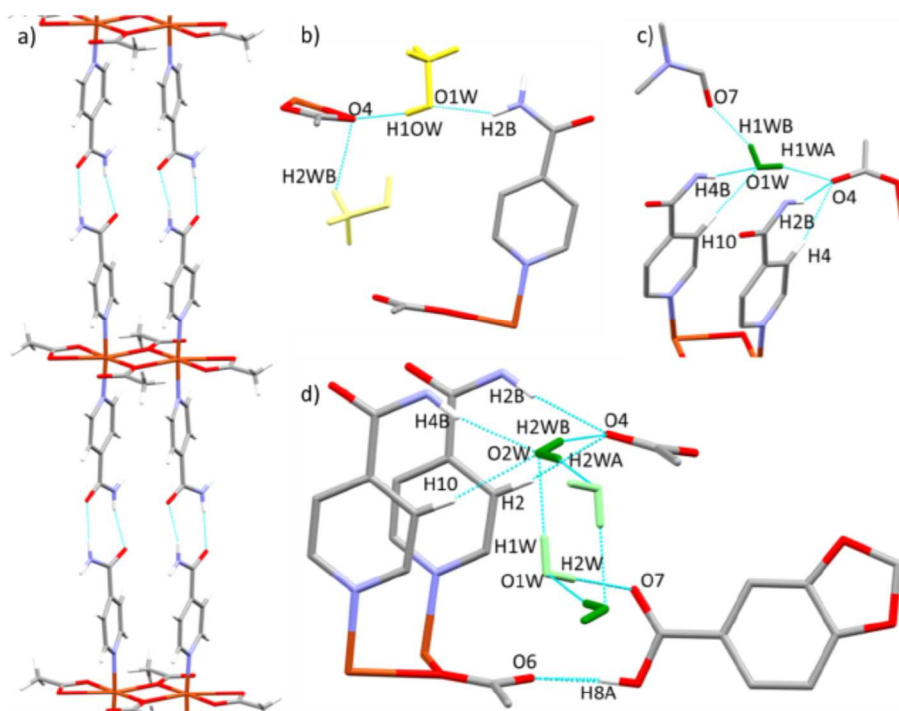


Figure 2. **a.** Representation of the supramolecular 1D expansion promoted by the Isn ligand present in compounds **2a-4a**. **b.** Intermolecular interactions generated by the MeOH occluded molecules (yellow and light yellow) present in **2a**. **c.** Intermolecular interactions generated by the dmf and H₂O (green) occluded molecules present in **3**. **d.** Intermolecular interactions generated by the H₂O (green and light green) and HPip occluded molecules present in **4a**.

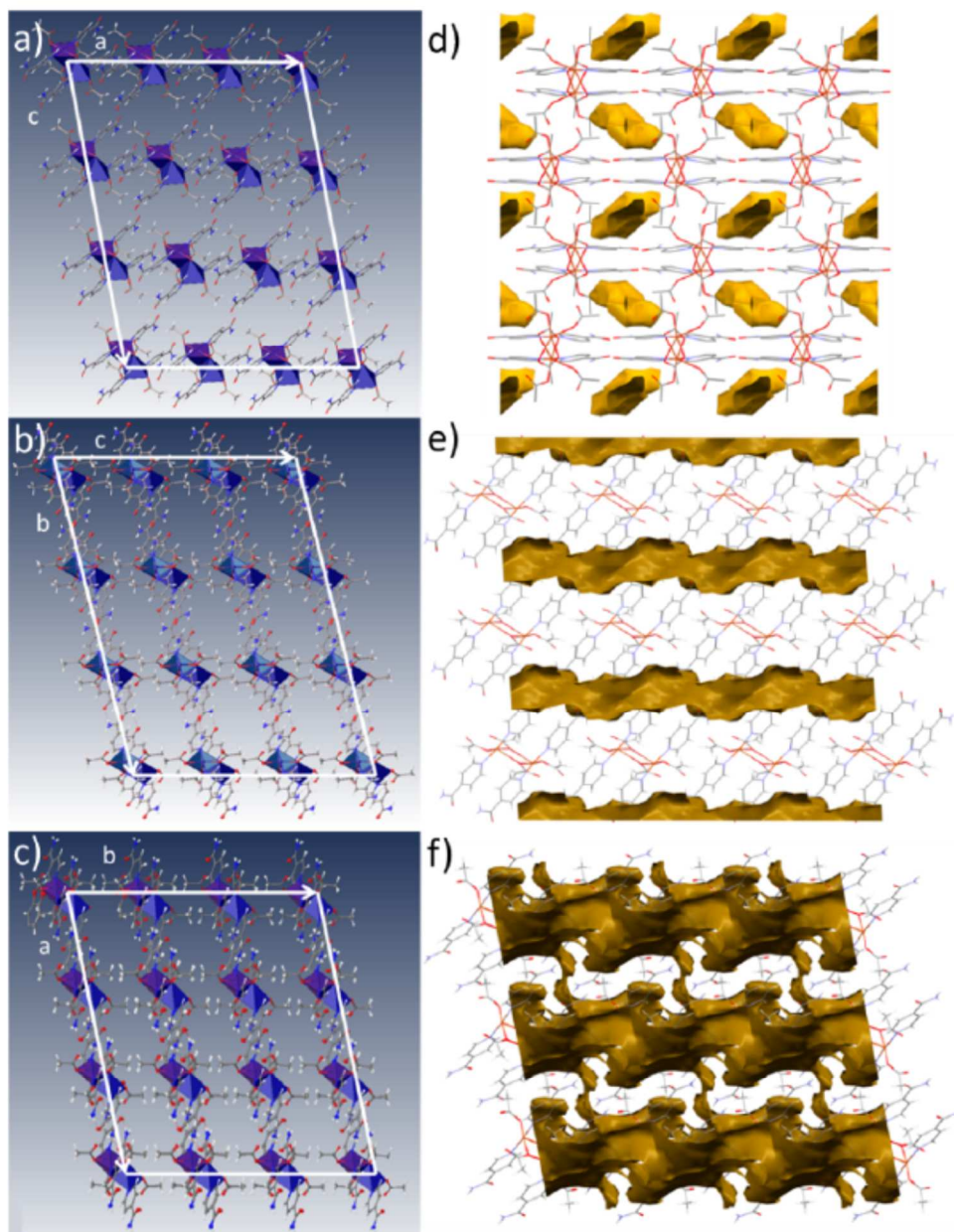


Figure 3. Representation of the 2D layers of compounds **a. 2a**; **b. 3**; and 3D net of **c. 4a**. Voids representation of the solvent occluded molecules of compounds **d. 2a**; **e. 3**; and **f. 4a**.

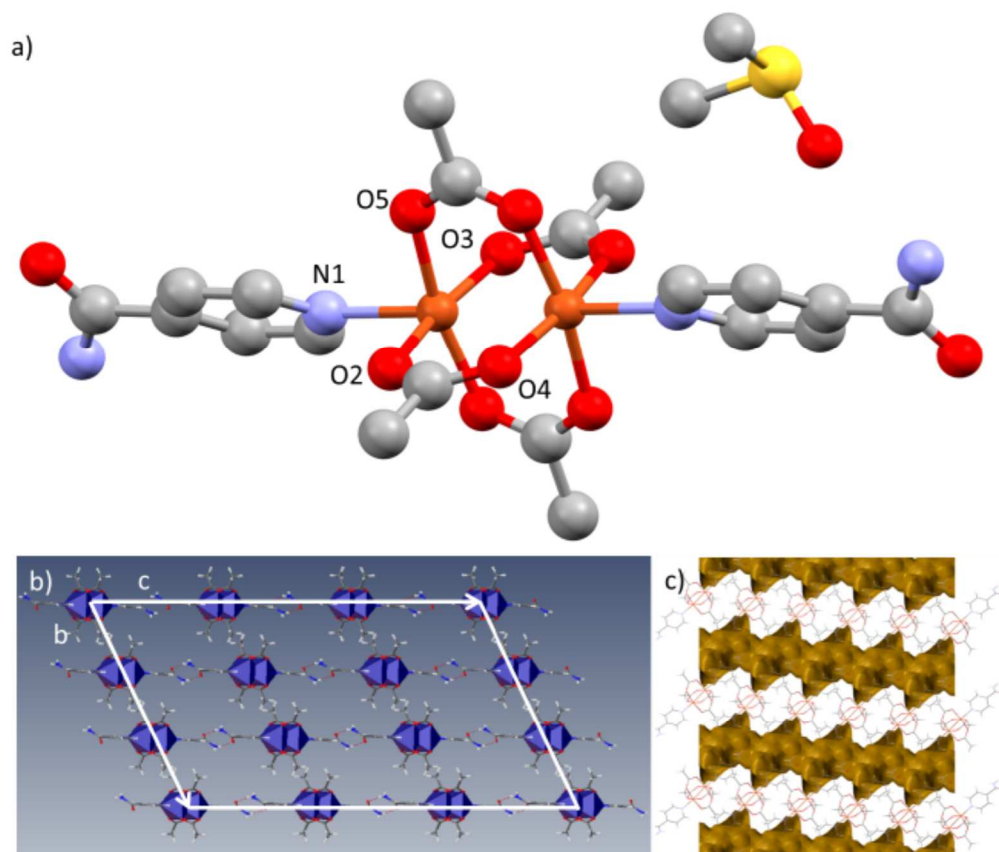


Figure 4. **a.** Representation of the molecular structure of **5**. Hydrogen atoms are omitted for clarity. **b.** 2D supramolecular expansion of **5** through the $\text{Isn}\cdots\text{Isn}$ interaction. **c.** Voids representation of the space occupied by the dmsoccluded molecules.

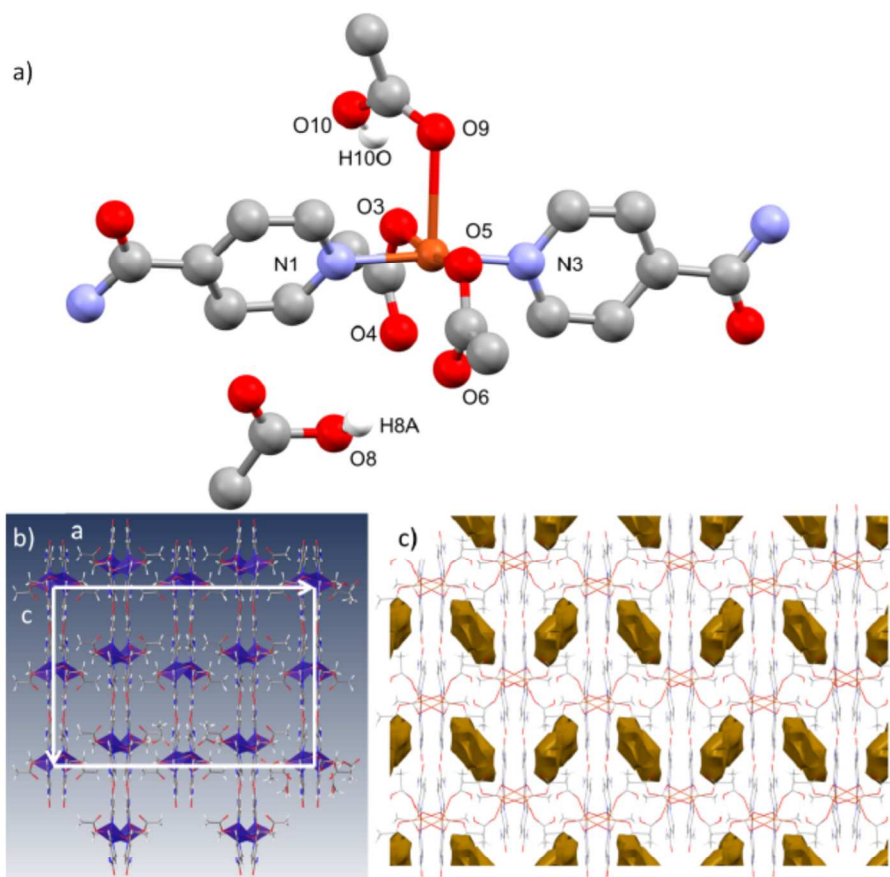


Figure 5. **a.** Representation of the molecular structure of **6**. Only hydrogen atoms of the HOAc units are present for clarity. **b.** 2D supramolecular expansion of **6** through the Isn...Isn and Isn...OAc interactions. **c.** Voids representation of the space occupied by the HOAc occluded molecules.

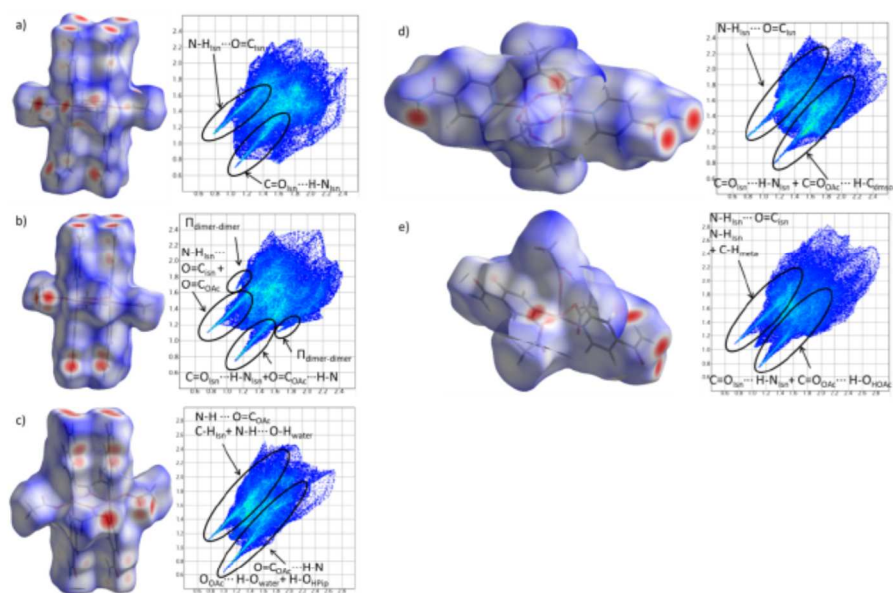


Figure 6. d_{norm} representation of the Hirshfeld surface and Fingerprint plot of compounds a. 2a. b. 3. c. 4a. d. 5. e. 6.

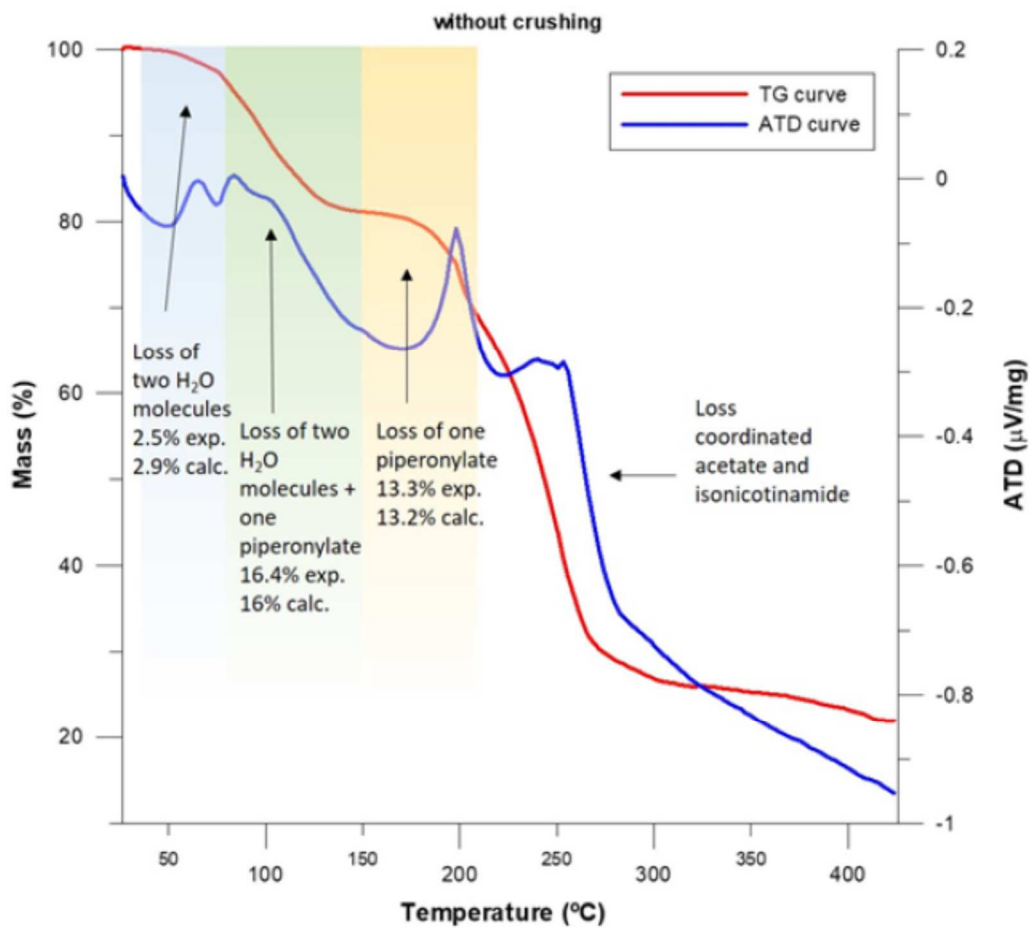


Figure 7. TG/DTA of compound **4a**.

Table 2. Distances [Å] and angles (°) related to hydrogen bond interactions and $\pi \cdots \pi$ interactions present in complexes **2a-4a**

2a	H...A (Å)	D...A (Å)	D-H (Å)	>D-H...A (°)
N2-H2A...O2	2.037(7)	2.888(7)	0.880(7)	162.32(7)
N2-H2B...O1W	2.039(7)	2.848(7)	0.880(7)	152.36(7)
N4-H4A...O1	2.041(7)	2.921(7)	0.880(7)	177.31(7)
N4-H4B...O6	2.039(7)	2.853(7)	0.880(7)	153.32(7)
O1W-H1OW...O4	1.967(7)	2.736(7)	0.783(7)	167.13(7)
C2H-H2WB...O4	2.399(7)	3.177(7)	0.980(7)	136.03(7)
C2H-H2WB...O3	3.124(7)	4.036(7)	0.980(7)	155.43(7)
$\pi \cdots \pi^i$	3.7412(7)			
3	H...A (Å)	D...A (Å)	D-H (Å)	>D-H...A (°)
N2-H2A...O2	2.010(3)	2.890(3)	0.880(3)	176(3)
N2-H2B...O4	2.010(4)	2.943(4)	0.880(4)	161(4)
N4-H4A...O1	2.050(3)	2.923(3)	0.880(3)	170(3)
N4-H4B...O1W	2.180(4)	3.043(4)	0.880(4)	168(4)
O1W-H1OW...O4	2.050(5)	2.827(3)	0.810(5)	162(5)
O1W-H1WB...O7	2.040(5)	2.760(4)	0.780(5)	153(5)
$\pi \cdots \pi^{ii}$	3.6220(16)			
$\pi \cdots \pi^{iii}$	3.6219(17)			
4a	H...A (Å)	D...A (Å)	D-H (Å)	>D-H...A (°)
N2-H2A...O2	2.020(2)	2.880(2)	0.880(2)	167(2)
N2-H2B...O4	2.18(2)	3.031(2)	0.880(2)	162(2)
N4-H4A...O1	2.06(2)	2.930(2)	0.880(2)	170(2)
N4-H4B...O2W	2.17(2)	3.036(2)	0.880(2)	167(2)
O1W-H1W...O2W	2.07(3)	2.902(2)	0.840(3)	172(3)
O1W-H2W...O7	1.87(3)	2.735(2)	0.870(3)	174(3)
O2W-H2WA...O1W	2.01(3)	2.805(2)	0.810(3)	168(3)
O2W-H2WB...O4	1.98(3)	2.797(2)	0.840(3)	166(3)
O8-H8A...O6	1.76(2)	2.621(2)	0.860(2)	173.5(19)
$\pi \cdots \pi^{iv}$	3.6682(11)			

i: $C_6(N1C1C2C3C4C5) \cdots C_6(N3C7C8C9C10C11)$. ii: $C_6(N1C1C2C3C4C5) \cdots C_6(N3C7C8C9C10C11)$. iii: $C_6(N3C7C8C9C10C11) \cdots C_6(N1C1C2C3C4C5)$. iv: $C_6(N1C1C2C3C4C5) \cdots C_6(N3C7C8C9C10C11)$.

+

Table 3. Intermolecular interactions comparison between compound **2a** and reported complex by Aakeröy *et al.* [26]

2a	H...A (Å)	D...A (Å)	D-H (Å)	>D-H...A (°)
O1W-H1OW...O4	1.967(7)	2.736(7)	0.783(7)	167.13(7)
C2H-H2WB...O4	2.399(7)	3.177(7)	0.980(7)	136.03(7)
C2H-H2WB...O3	3.124(7)	4.036(7)	0.980(7)	155.43(7)
[Cu(μ -OAc)(OAc)(Isn) ₂] ₂ ·2.5MeOH [26]	H...A (Å)	D...A (Å)	D-H (Å)	>D-H...A (°)
O1S-H1S...O42	1.95	2.754(3)	0.83	162.2
C2S-H2SA...O42	2.689	3.162	0.970	110.50
C2S-H2SA...O41	3.254	4.059	0.970	141.50

Table 4. Bond distances (Å) and bond angles (°) of compound **5**

5			
<i>Bond length (Å)</i>			
Cu(1)-O(3)	1.9774(18)	Cu(1)-N(3)	2.0091(19)
Cu(1)-O(5)	1.9844(16)	Cu(1)-N(1)	2.0091(19)
Cu(1)-O(9)	2.486(2)		
<i>Bond angles (°)</i>			
O(4)-Cu(1)-O(5)#1	168.85(3)	O(4)-Cu(1)-N(1)	97.51(3)
O(4)-Cu(1)-O(3)#1	88.57(3)	O(5)#1-Cu(1)-N(1)	93.61(3)
O(5)#1-Cu(1)-O(3)#1	89.14(4)	O(3)#1-Cu(1)-N(1)	97.97(3)
O(4)-Cu(1)-O(2)	90.22(4)	O(2)-Cu(1)-N(1)	93.01(3)
O(5)#1-Cu(1)-O(2)	89.96(4)	O(4)-Cu(1)-Cu(1)#1	85.00(2)
O(3)#1-Cu(1)-O(2)	169.02(3)		

Table 5. Distances [Å] and angles (°) related to hydrogen bond interactions and C-H...O interaction present in complex **5**

5	H...A (Å)	D...A (Å)	D-H (Å)	>D-H...A (°)
N2-H2A...O1	2.050(1)	2.905(1)	0.880(1)	163.01(1)
N2-H2B...O6	2.040(1)	2.890(1)	0.880(1)	162.01(1)
C11-H11A...O3	2.358(1)	3.314(1)	0.980(1)	164.88(1)

Table 6. Bond distances (Å) and bond angles (°) of compound 6

6			
<i>Bond length (Å)</i>			
Cu(1)-O(3)	1.9774(18)	Cu(1)-N(3)	1.9845(19)
Cu(1)-O(5)	1.9844(16)	Cu(1)-N(1)	2.0091(19)
<i>Bond angles (°)</i>			
O(3)-Cu(1)-O(5)	169.36(7)	O(5)-Cu(1)-N(3)	91.12(8)
O(3)-Cu(1)-N(3)	91.60(8)	O(5)-Cu(1)-N(1)	89.66(7)
O(3)-Cu(1)-N(1)	89.05(8)	N(3)-Cu(1)-N(1)	172.13(8)

Table 7. Intra- and Intermolecular interactions comparison between compound 6 and reported complex by Aakeröy *et al.* [26]

6	H...A (Å)	D...A (Å)	D-H (Å)	>D-H...A (°)
N2-H2A...O2	2.070(3)	2.931(3)	0.880(3)	166.02(7)
O8-H8A...O4	2.010(3)	2.644(3)	0.840(3)	131.26(4)
O10-H10O...O3 ⁱ	1.932(3)	2.637(3)	0.840(3)	140.88(7)
[Cu(OAc) ₂ (HOAc)(Isn) ₂]-HOAc [26]	H...A (Å)	D...A (Å)	D-H (Å)	>D-H...A (°)
N27-H27A...O17	2.20(3)	2.940(3)	0.74(3)	173(3)
O61-H61...O32	1.82	2.649(2)	0.83	173.0
O51-H51...O31 ⁱ	1.81	2.634(3)	0.83	170.4

i: intramolecular interaction

Table 8. Distances (Å) and angles (°) related to hydrogen bond interactions for compound 6

5	H...A (Å)	D...A (Å)	D-H (Å)	>D-H...A (°)
N4-H4A...O1	1.970(3)	2.845(3)	0.880(3)	171.61(7)
N2-H2A...O2	2.070(3)	2.931(3)	0.880(3)	166.02(7)
N2-H2B...O5	2.090(3)	2.897(3)	0.880(3)	151.23(7)
N4-H4B...O6	2.010(3)	2.868(3)	0.880(3)	164.49(7)
O8-H8A...O4	2.010(3)	2.644(3)	0.840(3)	131.26(4)
C10-H10...O6	2.300(3)	3.237(3)	0.950(3)	167.95(8)